Featureless Boson States with PEPS

Brayden Ware

August 2014

The proposed featureless boson insulator state has a wavefunction given by

$$|\psi\rangle = \prod_R \sum_{i \in R} b_i^\dagger |0\rangle \tag{1}$$

where R refers to each hexagonal plaquette of a honeycomb lattice, and $i \in R$ referes to the honeycomb sites adjacent to the plaquette R. It has been argued in [2] that this state represents a featureless Mott insulating phase of bosons on the honeycomb lattice.

Three variations:

- *Soft-core boson*

  This is the usual boson operator, which acts on the on-site boson number basis

  $$b^\dagger |N\rangle = \sqrt{N+1}\,|N+1\rangle$$

  with the commutation relations

  $$[b_i, b_j^\dagger] = \delta_{ij}.$$

  The on-site Hilbert space $\mathbb{H} = \text{span}(|N\rangle, N \in \mathbb{Z})$ is infinite-dimensional; but because each vertex is attributed at most one boson from each of its adjacent hexagons, the state lives in the subspace with at most 3 bosons on each site. The on-site Hilbert space can be truncated to 4-dimensions, where the boson creation operator is represented as

  $$b^\dagger = \begin{pmatrix} 0 & 0 & 0 & 0 \\ 1 & 0 & 0 & 0 \\ 0 & \sqrt{2} & 0 & 0 \\ 0 & 0 & \sqrt{3} & 0 \end{pmatrix},$$

- *Hard-core boson*

  This is the state obtained by taking the soft-core boson state and projecting on every site to the subspace of at most 1 boson on each site. Because of this projection, the on-site Hilbert space can be taken to be the 2-dimensional subspace $\mathbb{H} = \text{span}(|0\rangle, |1\rangle)$, with the boson creation operator represented on this subspace as:

  $$b^\dagger = \begin{pmatrix} 0 & 0 \\ 1 & 0 \end{pmatrix}$$

  Note that the boson operator restricted to this subspace clearly does not satisfy the usual boson commutation relations.

- *Large-N boson and other variations*

  A different wavefunction can be produced by instead starting with N bosons on each site before applying the plaquette boson creation operators - instead of with 0 bosons as above:

$$|\psi\rangle = \prod_R \sum_{i \in R} b_i^\dagger \, |N\rangle \, .$$

  This would be a candidate wavefunction for a incompressible state with boson density $N + \frac{1}{2}$ per site. We will argue that wavefunctions with different N can be smoothly connected without a phase transition, so we will not need to study the physics of each independently.

  The on-site Hilbert space is again effectively 4-dimensional: $\mathbb{H} = \text{span}(|N\rangle, |N+1\rangle, |N+2\rangle, |N+3\rangle)$. On this truncated Hilbert space the boson creation operator is represented as

$$b^\dagger = \begin{pmatrix} 0 & 0 & 0 & 0 \\ \sqrt{N+1} & 0 & 0 & 0 \\ 0 & \sqrt{N+2} & 0 & 0 \\ 0 & 0 & \sqrt{N+3} & 0 \end{pmatrix}$$

  In the limit N becomes very large,

$$\frac{b^\dagger}{\sqrt{N+1}} = \begin{pmatrix} 0 & 0 & 0 & 0 \\ 1 & 0 & 0 & 0 \\ 0 & \sqrt{1+\frac{1}{N+1}} & 0 & 0 \\ 0 & 0 & \sqrt{1+\frac{2}{N+1}} & 0 \end{pmatrix} \approx \begin{pmatrix} 0 & 0 & 0 & 0 \\ 1 & 0 & 0 & 0 \\ 0 & 1 & 0 & 0 \\ 0 & 0 & 1 & 0 \end{pmatrix}$$

  The $\sqrt{N+1}$ factor only changes the norm of the wavefunction, which is of no concern. After rescaling, all of these wavefunctions can be generated using Equation 1 with the replacement

$$b^\dagger = \begin{pmatrix} 0 & 0 & 0 & 0 \\ 1 & 0 & 0 & 0 \\ 0 & \sqrt{2}b_1 & 0 & 0 \\ 0 & 0 & \sqrt{3}b_2 & 0 \end{pmatrix} \tag{2}$$

  where $b^\dagger$ acts on a dimension 4 Hilbert space at each site with appropriate values of b_1 and b_2.

Similarly, starting with N bosons at each site, but using the boson annhilation operator b_i in place of the boson creation operator $b_i^\dagger$ in Equation 1 gives a different family of wavefunctions. These can be represented in the form of Equation 2.

Using instead the languague of spin, we can generate candidate wavefunctions for magnetization plateaus with half-integer magnetization $m =< S_z >= m_0 + \frac{1}{2}$ per site. This is done using a Hilbert space of spin-S at each site, starting each site in the state $|S^z = m_0\rangle$, and using spin raising/lowering operators $S_\pm$ in place of boson operators. These can be represented in the form of Equation 2 as well. In the limit $S \to \infty$, these states become equivalent to states generated by boson creation or annhilation operators.

The location of a of these states on the b_1-b_2 plane can be seen in Figure 1. We find that the correlation length stays bounded everywhere in this region $0 <= b_2 <= b_1$ and that it monotonically increases as you approach $b_1 = b_2 = 0$. This could justify using analytical techniques available at particular points in the plane - i.e., large-S expansion can be used at the large-N boson state (also described as $S- > \infty \; m_0 = 0$). Itamar's notes derive a rotor model that describes this point.

We will construct these wavefunctions as projected entangled pair states (PEPS) and the parameters b_1 and b_2 will appear in the site PEPS tensor. We then use these PEPS wavefunctions to numerically compute correlation functions and entanglement properties, focusing in-particular on the cases of the soft-core and hard-core bosons. After discussing these correlation functions in more detail, we argue that these states are in the same phase by looking at the correlation length as b_1 and b_2 continuously vary between the hard-core and soft-core boson states.

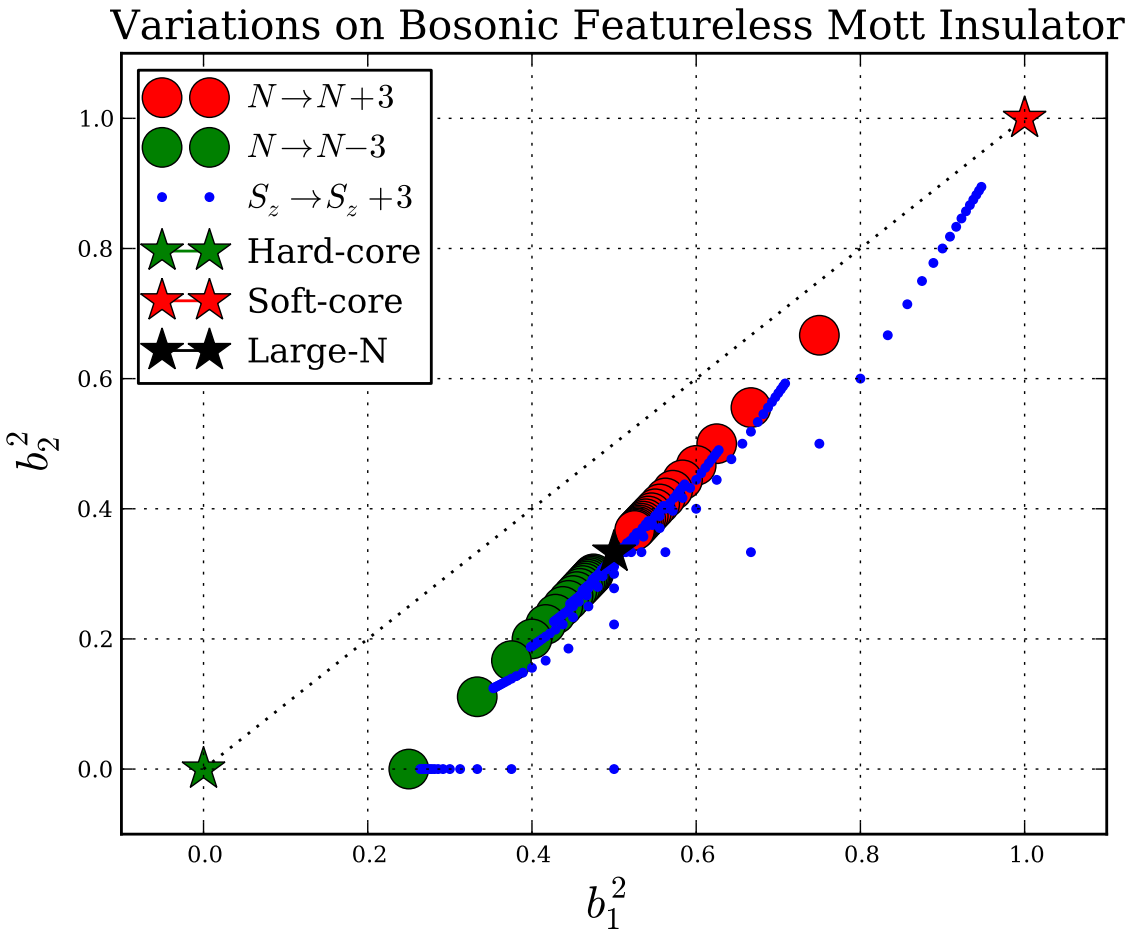

Figure 1: Plot of b_1 and b_2 for physically inspired variations on the featureless bosonic state. States colored red(green) - start with a vacuum of n bosons at each site and apply creation(destruction) operators. States colored blue have a spin-s Hilbert space on each site, start with all sites in the $|S_z = m\rangle$ state, and use spin-raising operators instead of boson-creation operators.

1 Methods

1.1 Making the PEPS

Each plaquette creation operator $\sum_{i\in R} b_i^\dagger$ can be written as a matrix product operator (MPO) acting on the six sites of a single hexagonal plaquette. By applying these MPOs for all plaquettes to the initial product state wavefunction $|\mathbf{0}\rangle$, we can construct a representation of the wavefunction as a PEPS with bond dimension 4 on the honeycomb lattice.

If we define the tensor

$$B^i_{\alpha\beta} = \left\{ \begin{array}{ll} \delta_{\alpha\beta} & : i = 0 \\ (b^\dagger)_{\alpha\beta} & : i = 1 \end{array} \right\}$$

in which the application of the creation operator is controlled by the state of the virtual qubit i, then the matrix elements of the plaquette boson creation operator can be specified by a trace over one virtual qubit per site x adjacent to the plaquette:

$$\left\langle \{\alpha_x\} \middle| \sum_{x\in R} b_x^\dagger \middle| \{\beta_x\} \right\rangle = \sum_{\{i_x\}} W^{i_0 i_1 i_2 \cdots} \prod_x B^{i_x}_{\alpha_x \beta_x} \tag{3}$$

The tensor $W^{i_0 i_1 i_2 i_3 i_4 i_5}$ which represents the state of the virtual qubits should be taken as the W-state,

$$W^{\{i_x\}} = \left\{ \begin{array}{ll} 1: & \sum_x i_x = 1 \\ 0: & \text{else} \end{array} \right\},$$

so that the trace results in 6 terms, each which acts as a creation operator on one site and identity on the other five sites.

The whole state can thus be represented as a contraction over all internal labels of a product of a W-tensor for every plaquette and a rank-4 site tensor D for each site, where

$$D_p^{i_0 i_1 i_2} = \sum_{\alpha\beta} B^{i_0}_{p\alpha} B^{i_1}_{\alpha\beta} B^{i_2}_{\beta 0}.$$

The internal labels i_0, i_1, i_2 connect the site to the adjacent plaquettes, and the label p represents the physical site Hilbert space. The coefficients are

$$\langle \{p_x\} | \psi \rangle = \sum_{\{i\}} \prod_R W^{\{i\}_R} \prod_x D^{\{i\}_x}_{p_x}. \tag{4}$$

This tensor network contraction scheme is different than PEPS because the W tensors exist not on the sites but the plaquettes - and sites are connected to adjacent plaquettes, not to adjacent sites. To rewrite the state in a PEPS representation, one should express the W-state as a matrix product state - i.e. as a tensor contraction of 6 tensors, each of which involving only one of the 6 virtual qubits i_j. These new tensors can be contracted into the on-site tensors, leaving only tensors on the sites. The bond dimension of the resulting PEPS representation is the square of the bond dimension of the MPS representation of the W-state.

A bond-dimension 2 representation of the W-state is given by

$$W^{i_0 i_1 i_2 i_3 i_4 i_5} = \sum_{abcde} W_1^{i_0 a} W_a^{i_1 b} W_b^{i_2 c} W_c^{i_3 d} W_d^{i_4 e} W_e^{i_5 0},$$

where

$$W^{\{i_x\}}_{\{j_y\}} = \left\{ \begin{array}{ll} 1: & \sum_x i_x = \sum_y j_y \\ 0: & \text{else} \end{array} \right\},$$

and where each index takes values in $\{0, 1\}$.

This representation leads to a small bond dimension (4) for the PEPS. Exact computations quickly become intractable as the PEPS bond dimension grows, so the small bond dimension is essential for direct

computations of properties of the wavefunction. On the other hand, this representation does not respect the translational symmetry (or the bigger permutational symmetry) of the virtual qubits in the W-state, causing the PEPS representation of the boson state to not respect the point group symmetry of the honeycomb lattice. The smallest known bond dimension of a translationally symmetric representation of the W-state on six sites is 6 [3], which would lead to a bond dimension 36 for the PEPS.

1.2 Cyinder PEPS

We measure correlations in this wavefunction by using methods designed for infinite length translationally symmetric MPS.

In order to facilitate this, the honeycomb lattice on a plane has been periodically identified, yielding a honeycomb lattice on an infinite cylinder. The identification used for the calculations below results in the zig-zag configuration, pictured in figure 14, although an armchair or various chiral configurations of the lattice on the cylinder are possible as well. Each identification will break different space-group symmetries of the original planar honeycomb lattice.

After the periodic identification, blocking each slice of the cylinder leads formally to an MPS with physical Hilbert space dimension p^{2L} and virtual bond dimension d^L, where p is the physical dimension of the original on-site Hilbert spaces, d is the bond dimension of the PEPS, and L is the circumference of the cylinder measured using the number of bonds cut. We will call the site tensor for this MPS A^p_{ab}.

The double tensor $(\mathbb{E}_I)_{AB} = (A^p_{a_1b_1})^* A^p_{a_2b_2}$ of this MPS is the key object of this method of computing expectation values. I will refer to it to below as the transfer matrix. Lets assume for sake of discussion that it is normalized to have largest eigenvalue 1, with eigenvectors $|v)_B$ on the right and $(v|_A$ on the left.

The tensor network contraction for the expectation value of an operator O is represented by

$$\langle\psi|O|\psi\rangle = ...\mathbb{E}_I\mathbb{E}_I\mathbb{E}_O\mathbb{E}_I\mathbb{E}_I...$$

We could carry out this calculation by cutting the infinite contraction off after a fixed finite distance and setting boundary conditions for the open ends. However, the application of the transfer matrix many times will converge (exponentially) to the largest eigenvector starting with *any* boundary condition. We avoid finite size corrections in the length of the cylinder by directly using the largest eigenvector of the transfer matrix.

$$\langle\psi|O|\psi\rangle = (v|_A \, (\mathbb{E}_O)_{AB} \, |v)_B$$

Similarly the tensor network contraction for a two point correlation function is represented by

$$\langle\psi|O_0O_x|\psi\rangle = (v| \, \mathbb{E}_{O_0}(\mathbb{E}_I)^x\mathbb{E}_{O_x} \, |v) \, .$$

1.3 Numerical Implementation

The eigenvectors $|v)_B$ and $(v|_A$ are computed exactly using a numerical diagonalization scheme (Arnoldi) targeted at finding the largest eigenvalue of a matrix.

Since the dimensions of the tensor $(\mathbb{E}_I)_{AB}$, are $(d^2)^L \times (d^2)^L$- where for the calculations below, $d = 2$ and L ranges up to 8 - the exponential growth in matrix size strains computer memory, and the exponential growth in diagonalization time strains patience.

Fortunately, for Arnoldi, as in most numerical diagonalization schemes, the double tensor need not be computed explicitly - instead, only a method to compute the action of that double tensor on a vector is defined and passed to the diagonalization code. The memory requirements are reduced from the size of the matrix, d^{4L} complex numbers, to the size of the vectors d^{2L} complex numbers, at a cost in runtime for computing the action of the matrix.

In order to reach larger sysetm sizes in a reasonable amount of time, it was necessary to make full use of the on-site symmetries of the MPS: a $U(1)$ boson number conservation symmetry, inherited from the boson $PEPS$, and momentum conservation for translations around the cylinder. A well known fact of MPS is that these physical symmetries generically translate into symmetries of the double tensor $\mathbb{E}_I$ acting on the virtual, doubled, edge. This means that transfer matrix is block diagonal in the appropriate basis. This asymptotic size of the largest block grows as $\frac{d^{2L}}{L^{3/2}}$.

2 Data and Analysis

2.1 The nature of MPS Correlation Functions

Formally expanding $\mathbb{E}_{O_x}|v)$ in terms of a basis of right eigenvectors of $\mathbb{E}_I$ shows that the correlation function

$$\langle\psi|O_0O_x|\psi\rangle = (v|\,\mathbb{E}_{O_0}(\mathbb{E}_I)^x\mathbb{E}_{O_x}\,|v)\,. \tag{5}$$

will evaluate to a sum of decaying exponentials

$$\langle\psi|O_0O_x|\psi\rangle = C_1 + C_2e^{-E_2x} + C_3e^{-E_3x}...$$

where $\lambda_1 = e^{-E_1} = 1, \lambda_2 = e^{-E_2}, ...$ are the ordered (by decreasing absolute value) eigenvalues of $\mathbb{E}_I$.

Therefore connected correlation functions - where the constant term C_1 is 0 - have correlation lengths bounded by $\xi = \frac{1}{E_2} = \frac{1}{\log|\frac{\lambda_1}{\lambda_2}|}$. In fact, the correlation length will be exactly $\xi = \frac{1}{E_2}$ unless the constant C_2 is 0 for symmetry reasons. The set $\xi_i = \frac{1}{E_i} = -\frac{1}{\log|\lambda_i|}$ represents a spectrum of all the possible correlation lengths of operators in this MPS representation. The eigenvalues λ_i need not be real, with non-zero phase corresponding to oscillatory behavior in the correlation functions.

Additional information can be gained by combining this argument with the on-site symmetries of the MPS. The smallest eigenvalue in each symmetry sector will give a correlation length bound for operators which create states in that symmetry sector, based on the inverse of the decay constant of the leading decaying exponential in the correlation function. Most operators in that symmetry sector will have exactly that correlation length, unless they manage to have the constant of the leading exponential be exactly 0, in which case the correlation length will be lower (but still the inverse of one of the eigenvalues in the spectrum).

For small L, we can diagonalize all of the symmetry sectors of $\mathbb{E}_I$, and plot the eigenvalues, as in figure 2. The y-coordinate of the points is $E_i = -\log|\lambda_i| = \frac{1}{\xi_i}$. The x-coordinate of the plots is the momentum sector, and the points are colored by boson number, the relevant U(1) charge. A few of the corresponding correlation lengths are labeled on the plot.

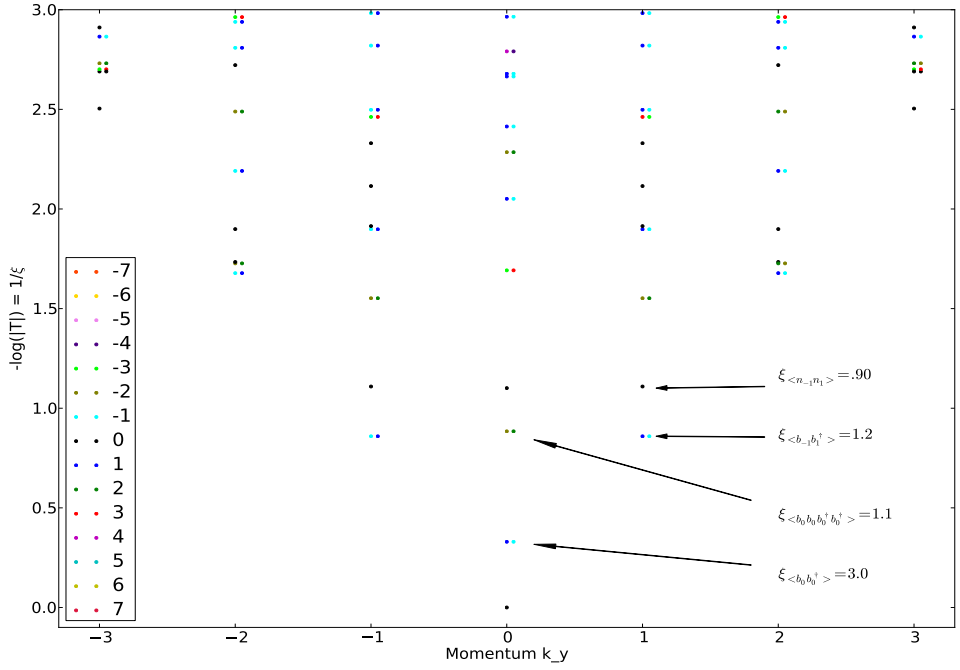

Figure 2: Spectrum of inverse correlation lengths for the soft-core boson state with L = 7. The annotations indicate the spectrum points with the quantum numbers appropriate for the boson correlation function $< b_k^\dagger b_{-k} >$ and the density correlation function $< n_k n_{-k} >$.

These plots give us a quick way to assess the correlation properties of the proposed bosonic states. However, the information they show is inherently one dimensional - they determine how the correlation functions behave asymptotically as you go down the length of the cylinder, not how it behaves at short distances or in the circumferential direction. These correlation lengths are subject to large finite size effects in the circumference of the cylinder. Furthermore, operators with the same quantum numbers can't be distinguished without more work.

In the next section, we will look at these transfer matrix spectrum plots and the correlation length bounds that they imply. Section 2.3 will look instead at the more detailed short distance correlation function data.

2.2 Correlation Bounds for Bosonic States

These plots show the lowest spectrum points, which correspond to the heighest weights of the transfer matrix, in more detail. First, the soft-core boson state is shown for multiple cylinder widths.

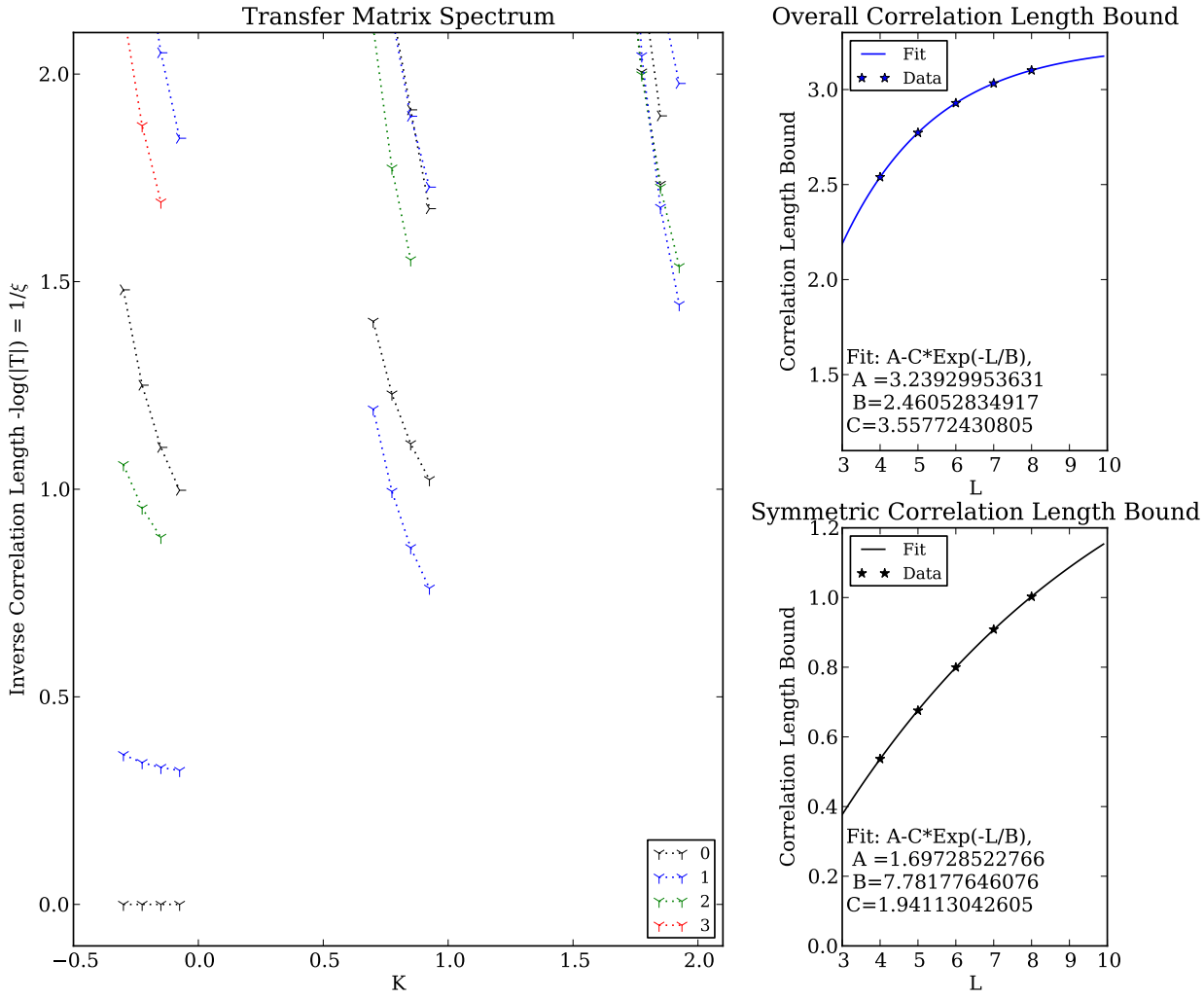

Figure 3: Lowest few eigenvalues of the transfer matrix spectrum for soft-core boson state shown for cylinder widths $L = 5, 6, 7, 8$. Color indicates boson number N; the degenerate spectum points at negative charge are suppressed from the plot. The data from the lowest non-zero eigenvalue occuring for $K = 0, N = 1$, and the $K = 0, N = 0$ eigenvalue are used to make the correlation length bounds shown on the right. Finite size extrapolation predicts that the correlation bound for all sectors is around 3.2, and for symmetric sectors is around 1.7, using a decaying exponential fit - but significant finite-size effects exist.

It is clear from this data that the overall correlation length bound has a finite limit, and thus all correlation functions will be gapped. Attempting to fit power law or logarithmically increasing functions to the correlation length data does not give good results, while the exponentially decaying fit function shown in Figure 3 fits well.

On the other hand, if we had found that the decay constants of the exponentials decreased to zero as the MPS bond-dimension increased, it could be that the actual correlation functions show power-law decay in the thermodynamic limit of an infinitely wide cylinder. This could not occur for a MPS product state limited to a fixed bond dimension, but it can occur for a PEPS with a finite-bond dimension, given the effective MPS bond dimension that grows with the circumference of the cylinder. Thus, a PEPS can represent a critical point with finite bond dimension, with the infinite correlation length detectable using finite-size scaling.

Given the strong finite-size corrections that appear - especially for the symmetric sector - the extrapolated correlation lengths shouldn't be taken as exact, just indicative of greater or less correlations.

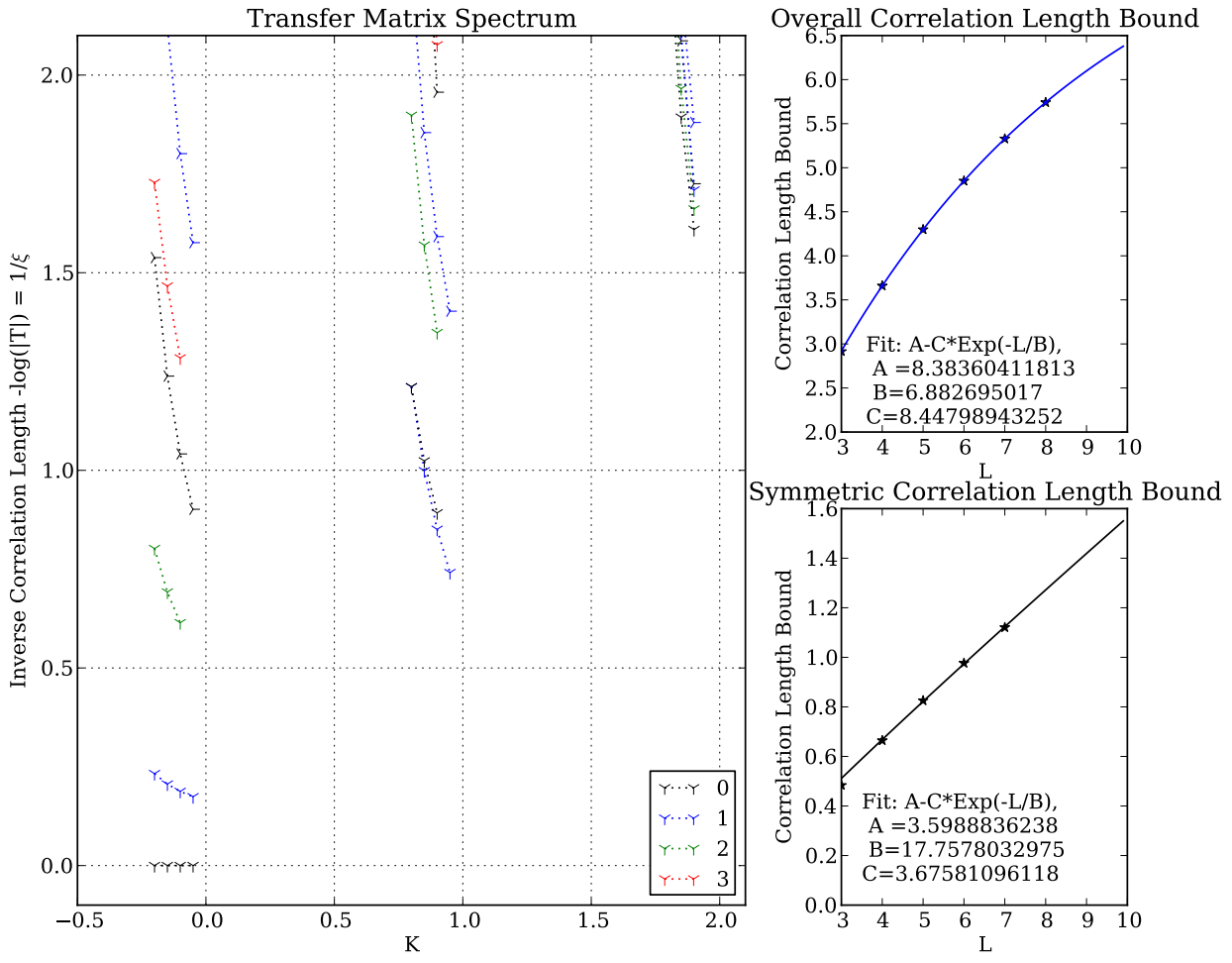

Figure 4: Same as Figure 3 but with the hard-core boson state instead. Finite size extrapolation shows that the correlation length bound for all sectors is around 8.4, and for symmetric sectors is around 3.6. Note the increase of correlation length over the soft-core boson states, as well as the increase in finite-size corrections.

The hard-core boson states had much larger correlations than the soft-core states, as shown in Figure 4. This may be unexpected. Applying the hard-core projection suppresses boson-number fluctuations, so naively it should move you further from the phase-transition to a superfluid, where boson-number fluctuations diverge.

This increase in correlations could be explained if applying the hard-core projection causes the system to pass through a phase transition. By continuously tuning the PEPS parameters b_1, b_2 from the soft-core

state with $b_1 = b_2 = 1$ to the hard-core state with $b_1 = b_2 = 0$, we found that the correlation length increases monotonically from the soft-core state to the hard-core state, as shown in Figure 5. This seems to rule out a phase transition as the explanation for the increase in correlations.

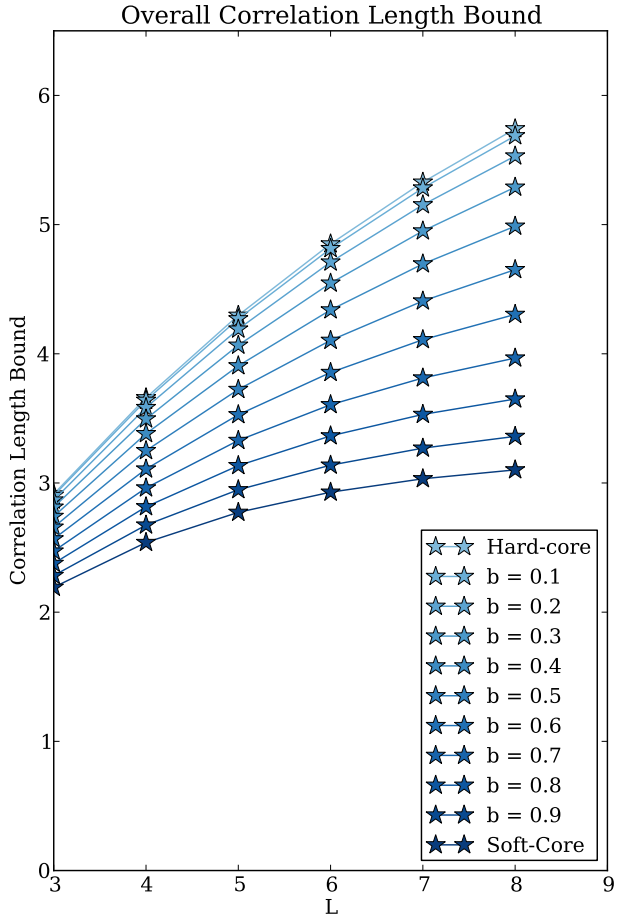

Figure 5: Correlation length bound when the PEPS parameters are tuned from the soft-core to the hard-core boson states along the line $b_1 = b_2 = b$. Correlation length monotonically increases as hard-core projection is applied.

2.3 Detailed Correlation Functions

Using Equation (5), the computed boson correlator $< b_x b_0^\dagger >$ and the density correlator $< n_x n_0 >$ are shown in Figures 16, 17, 18, and 19 in the Appendix.

The correlation maps confirm properties of the correlation functions predicted by the transfer matrix spectrum alone: that the correlation lengths increase with cylinder circumference L, that they increase as you tune from the the soft-core to the hard-core state, and that the density-density correlations are much more short-ranged than the hopping correlation functions.

While the correlation length determined from the asymptotic decay of the hopping is greater in the hard-core state in comparison to the soft-core state, the short distance hopping is actually much smaller. This short distance hopping is suppressed by the hard-core projection due to the lack of available states to hop into when neighboring sites are filled.

Another notable feature here is that the full point group symmetry of the honeycomb lattice is recovered at short distances in the correlation functions, despite not being a symmetry of the honeycomb on a cylinder

due to the periodic boundary conditions. If the state spontaneously breaks rotational symmetry in the thermodynamic limit, we would expect to instead see sensitivity to the boundary conditions at finite sizes.

The correlation functions are shown plotted versus distance along the cylinder in Figure 6. The minimum distance $d(x)$ along the cylinder for the points reachable by x applications of the transfer matrix is asymptotically $d(x) \approx 1.5x$, so one would expect the correlation length measured along the cylinder to be around 1.5 times the MPS correlation length.

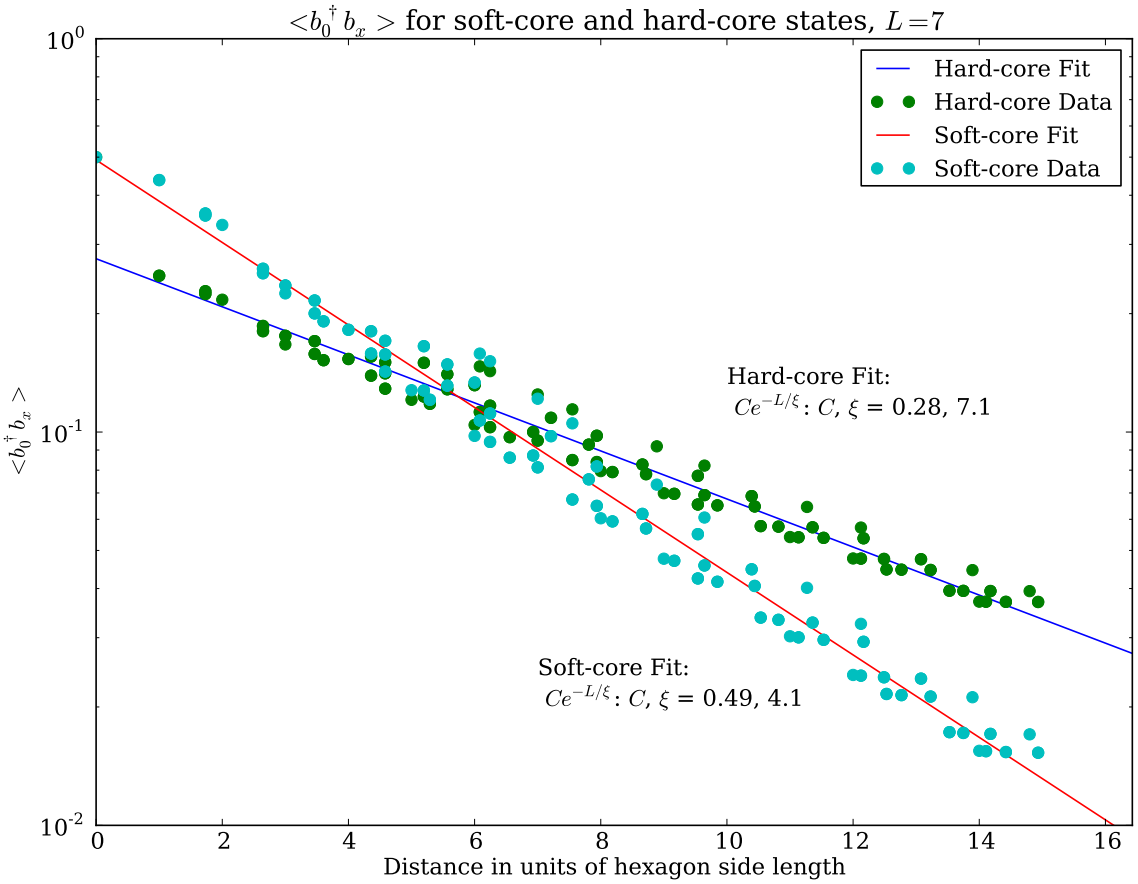

Figure 6: The correlation function $< b_x b_0^\dagger >$ shown on a log-scale for the hard-core and soft-core boson states. The distance d_x is computed using the shortest path along the cylinder and measured in units of the hexagon side length. Compare to the MPS correlation length 3.0 for the soft-core boson and 5.4 for the hard-core boson at $L = 7$.

2.4 Entanglement properties of the boson states

The eigenvector $|v)_B$ (and similarly the left eigenvector $(v|_A$) of the transfer matrix represents a density operator ρ_B on the Hilbert space of the virtual qubits at the right edge (left edge) of a half-infinite cylinder. (ρ_B is formed by reshaping $|v)_B$.) The spectrum of this density operator coincides with the reduced density matrix formed from the wavefunction on a fully infinite cylinder and tracing over all the degrees of freedom on half the cylinder. [1]

This density matrix ρ_B is Hermitian, positive semidefinite, and can be rescaled to have trace 1. It is also block-diagonal in the appropriate basis of boson number and transverse momentum eigenstates. The operator H_e satisfing $\rho_B = \exp -H_e$ is called the entanglement Hamiltonian, and its spectrum the entanglement spectrum. These spectra can be used to characterize long-range entanglement properties in

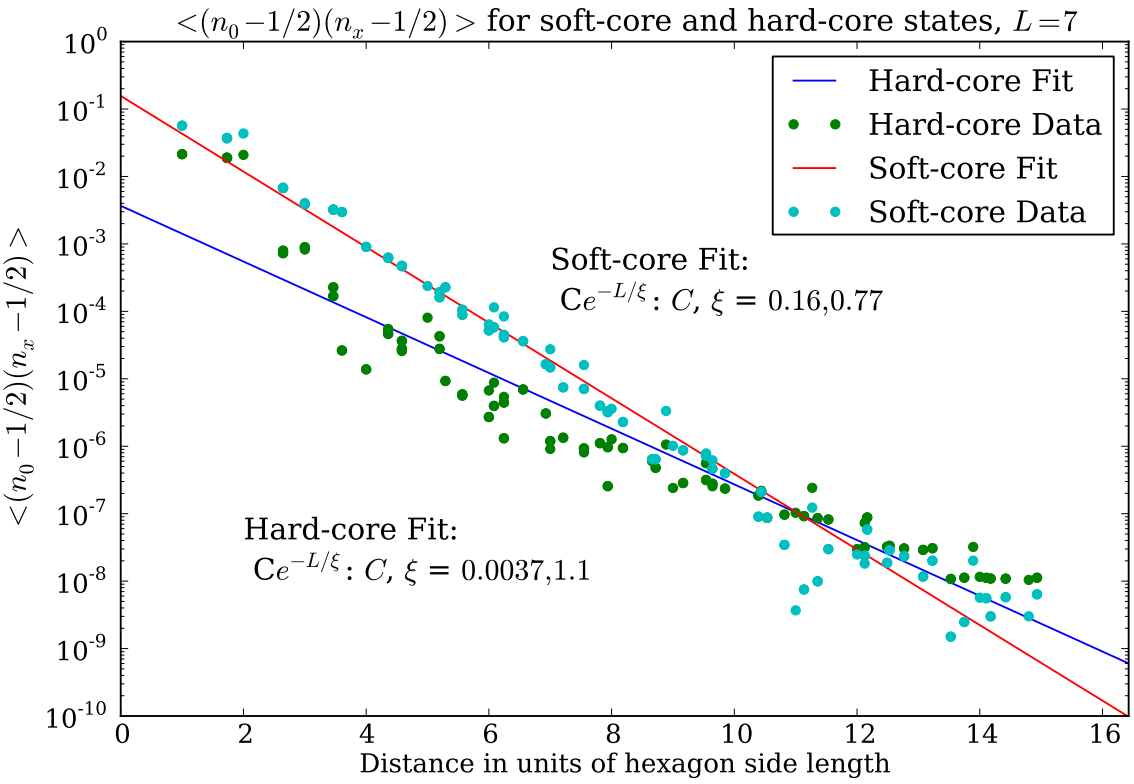

Figure 7: The absolute value of the connected density correlation function $|<(n_x-\frac{1}{2})(n_0-\frac{1}{2})>|$ shown on a log-scale for the hard-core and soft-core boson states. The correlation values are both positive and negative - an alternate version of this plot that shows the sign structure is in Figure 20. Compare to the symmetric MPS correlation length 0.9 for the soft-core boson and 1.1 for the hard-core boson at $L = 7$.

the states. In particular, topological order can sometimes be identified by a gapless spectrum and non-zero topological entanglement entropy, and symmetry protected topological order can sometimes be identified by a gapless spectrum appearing only if the entanglement cut respects the symmetry.

The plots in this section show the entanglement spectrum for the soft-core featureless boson state. The other states in the $b_1 - b_2$ plane have similar spectra. The eigenstates of the entanglement Hamiltonian - the Schmidt states - can be assigned a relative U(1) charge, which can be counted by adding contributions of $\pm\frac{1}{2}$ from each site in the virtual edge; this motivates an analogy to a spin chain with $S_z = \pm\frac{1}{2}$ per site. In the spin chain language, we will see that the entanglement Hamiltonian is an anisotropic gapless antiferromagnet with no magnetic field.

The full spectra for two different system sizes are shown in Figures 8 and 9. Like an antiferromagnet in zero field), the ground states have U(1) charge $e = 0$ for even numbers of sites or $e = \pm\frac{1}{2}$ for odd numbers of sites. The spectra are independently symmetric under charge conjugation and reversing the momenta parallel to the cut.

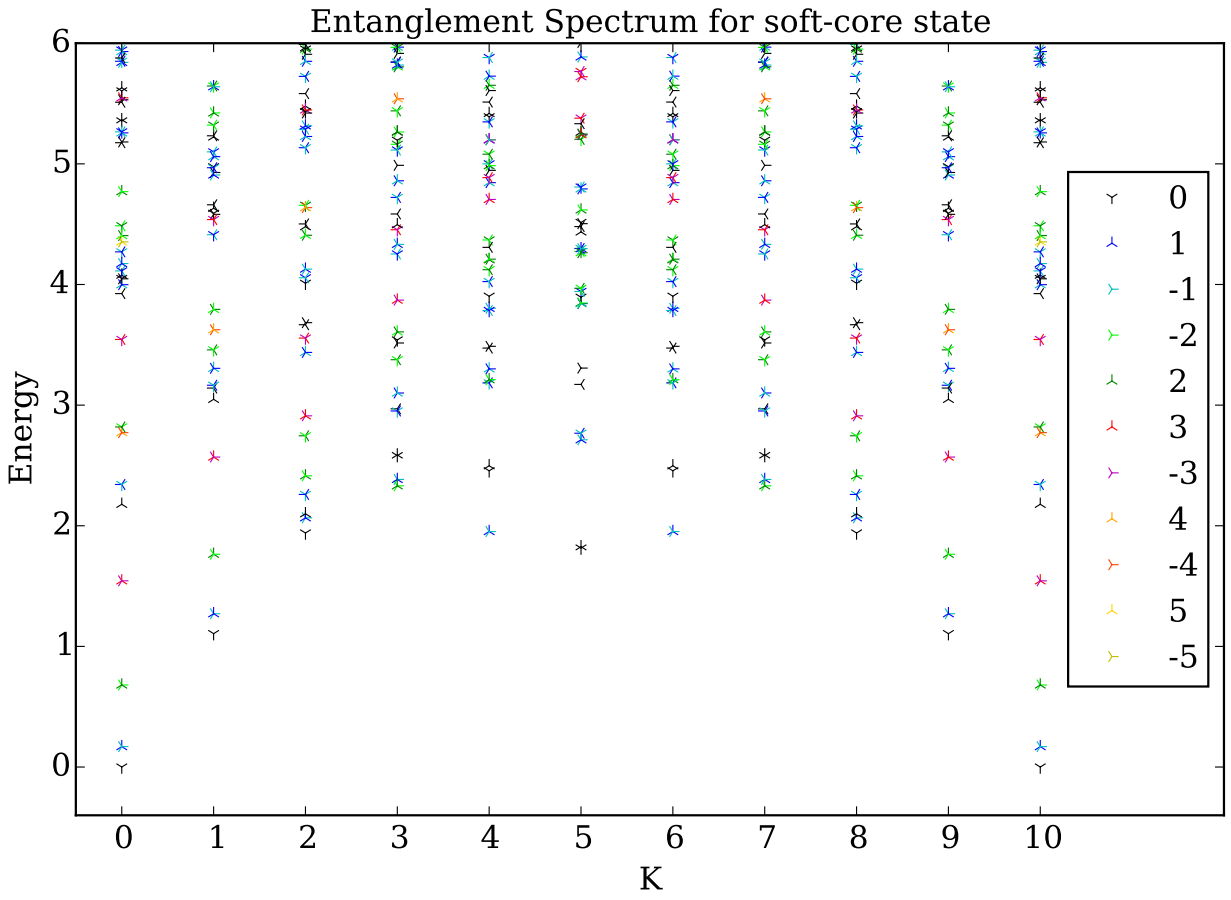

Figure 8: Full entanglement spectrum for the soft-core boson state on the $L = 10$ zig-zag edge cylinder. Scale set by making the density matrix have trace 1, i.e. $\sum_i \exp(-E_i) = 1$. The color represents a relative $U(1)$ charge - each edge site on the cut contributes $\pm\frac{1}{2}$. The spectra is symmetric under charge conjugation and/or reversing the momenta parallel to the cut, which leads to degeneracies for all states except the states with 0 charge.

By careful finite-size analysis of the low-energy entanglement spectrum of the soft-core boson state, we find that the spectrum can be consistently matched to the gapless spectrum of a compactified free boson, a CFT with central charge $c = 1$, in a way comparable to the spectra of a gapless antiferromagnet spin-chain.

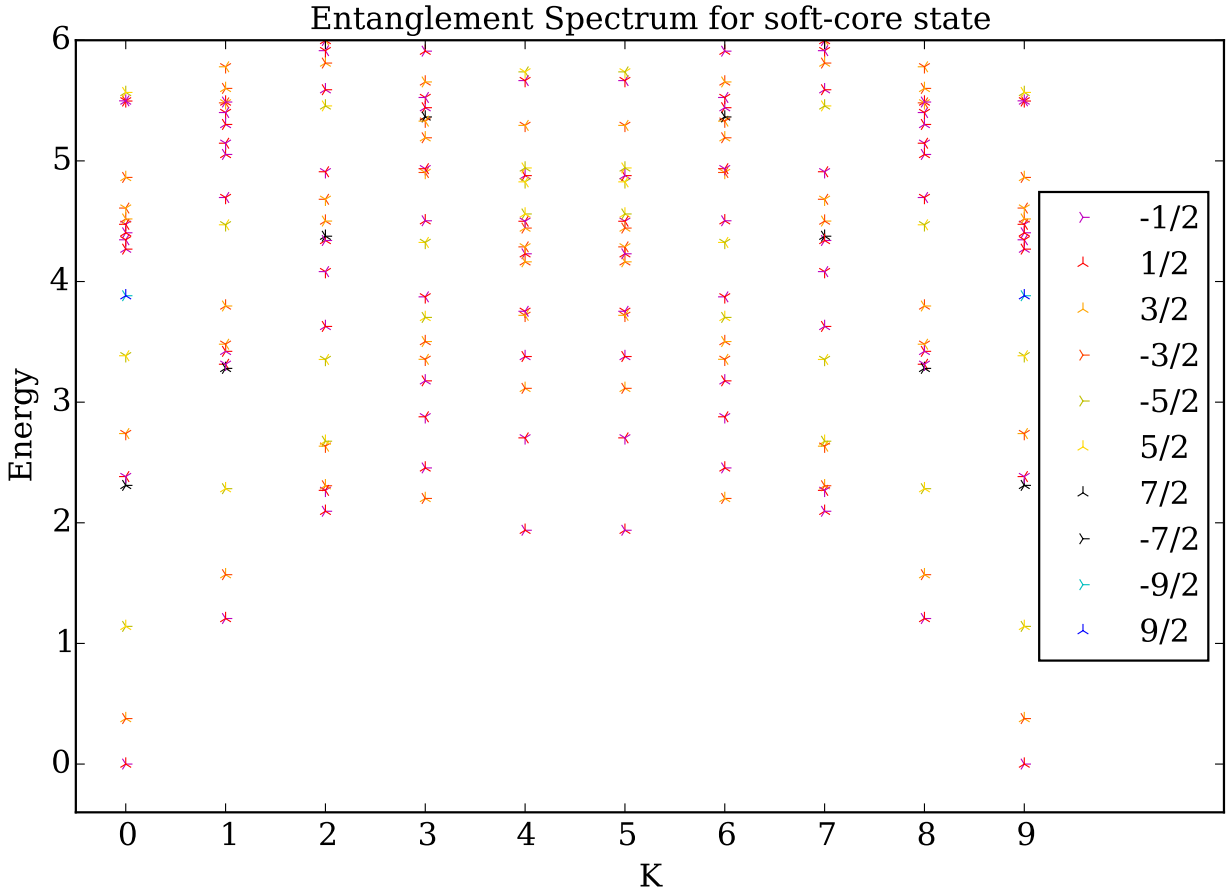

Figure 9: Full entanglement spectrum for the soft-core boson state on the $L = 9$ zig-zag edge cylinder. Scale set by making the density matrix have trace 1, i.e. $\sum_i \exp(-E_i) = 1$. The color represents a relative $U(1)$ charge - each edge site on the cut contributes $\pm\frac{1}{2}$. With an odd number of sites, the charge is half-odd-integer. The spectra is symmetric under charge conjugation and/or reversing the momenta parallel to the cut, leading to a double degeneracy for all states.

The evidence for gaplessness is shown in Figure 10 - a close-up of the lowest energy states near momentum 0 for several system sizes - and Figure 11 - fits for the scaling forms of the lowest collection of states.

All of the eigenstates with 0 momentum show $1/L$ scaling as would be expected in a gapless state. Eigenstates with other momenta should eventually show $1/L$ scaling, but might not at small system sizes. For example, a free gapless boson on L sites in periodic boundary conditions has a band of single particle eigenstates of the form $|\sin(\pi K/L)|$ with $K \in 0, 1, ...L-1$. For small system sizes, $\sin(\pi/L)$ deviates from $1/L$ scaling.

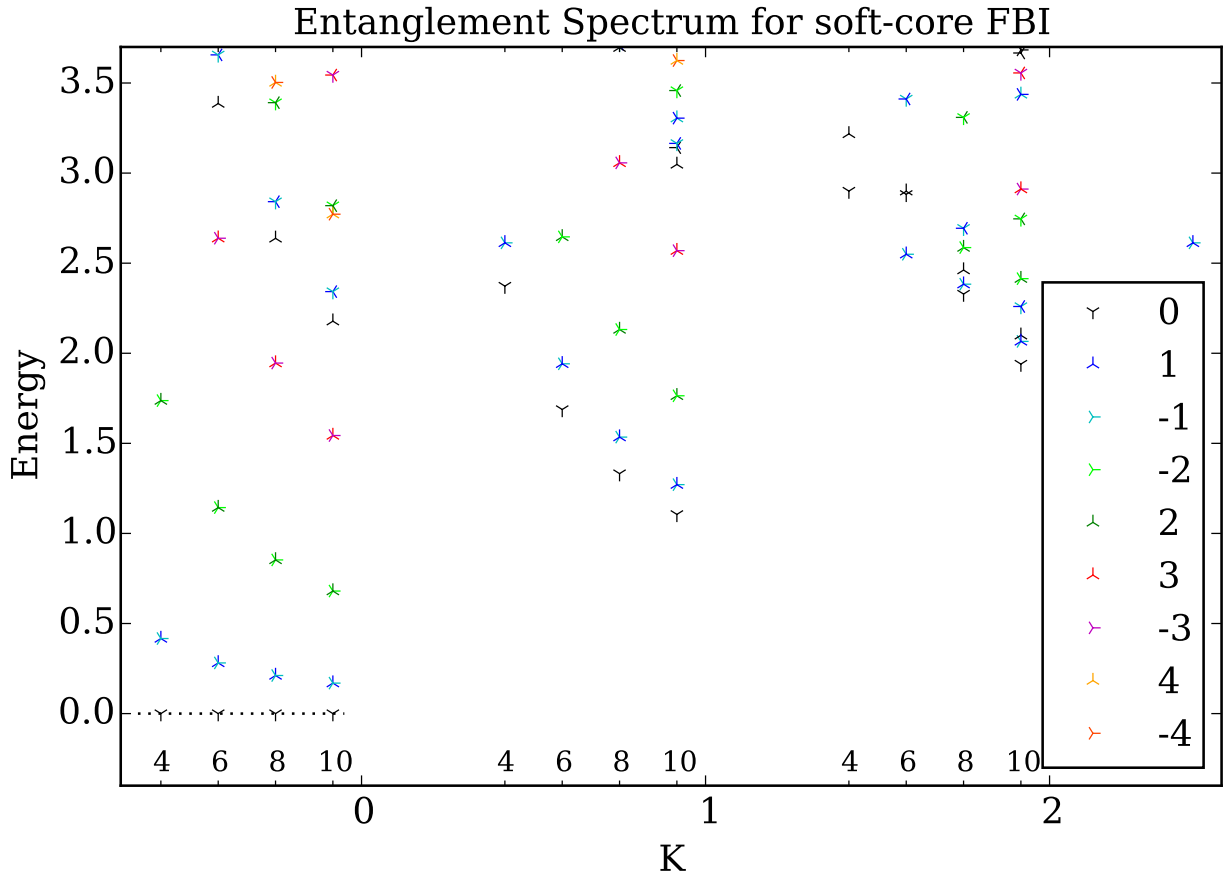

Figure 10: A close-up of the lowest energy states in Figure 8, shown at each momentum for system sizes $L = 4, 6, 8, 10$. The lowest few states above the ground state are fit to power laws in Figure 11.

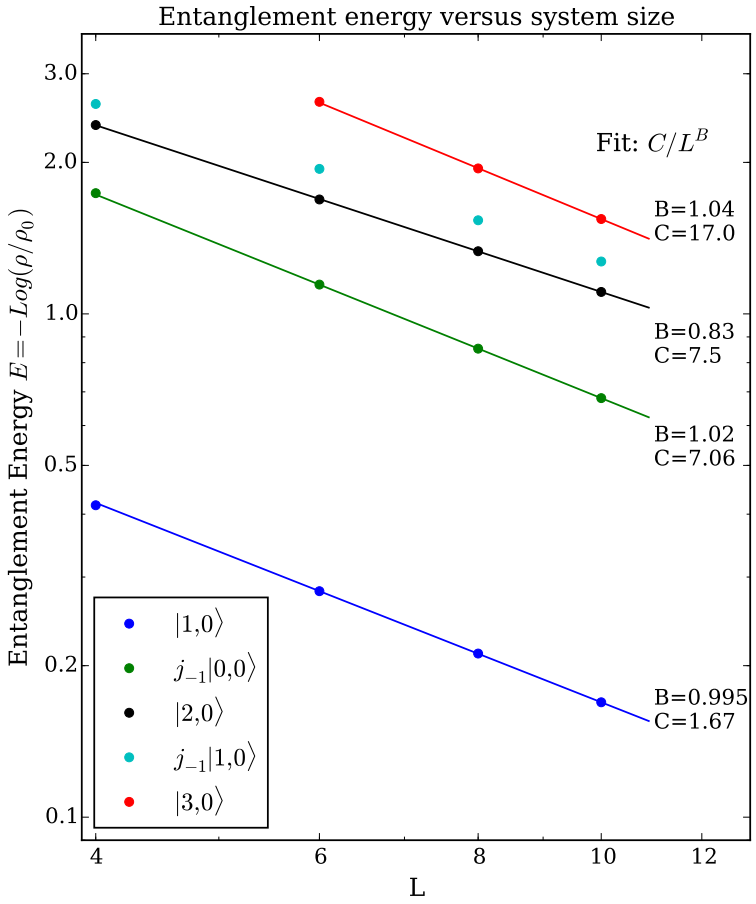

Figure 11: Power law fits for the lowest three states above the ground state at momentum zero and lowest two states at momentum 1 in Figure 10. The $1/L$ scaling is a signature of a gapless (entanglement) Hamiltonian. The labeling of the states $|e, m\rangle$ or $j_{-1}|e, m\rangle$ is explained in the CFT section below.

Since our Hamiltonian is gapless, we can try to describe it using a conformal field theory. A measurement of the central charge can be obtained by looking at the entanglement entropy within the ground state. The Cardy-Calabrese formula states that the entanglement entropy $S(x)$ for a region of size x on a system of size L with periodic boundary conditions is given by

$$S(x) = c/3 \log\left(\sin(\pi \frac{x}{L})\right) + const.$$

In figure 12 we show that $S(x)$ is described by the Cardy-Calabrese formula with $c = 1$.

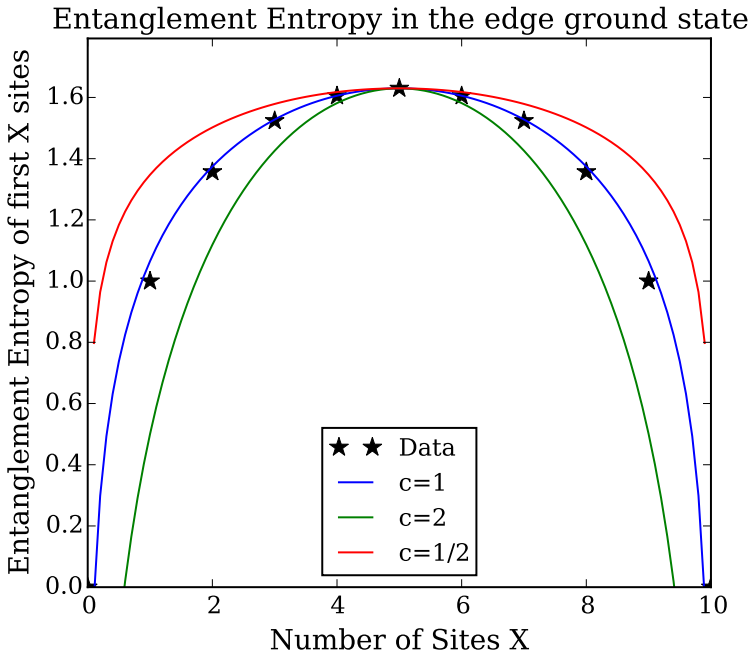

Figure 12: Entanglement entropy within the entanglement ground state of the soft-core boson state on 10 sites. For comparison, the Cardy-Calabrese formula $S(x) = c/3 \log \sin(\pi x/L) + const.$ is shown with $c = \frac{1}{2}, 1,$ and 2, with the *const.* fixed by matching the maximum of the entanglement entropy data. $c = 1$ is a good fit.

2.5 Identifying the CFT

Given the $U(1)$ symmetry of the state and the central charge $c = 1$, the simplest conformal field theory that could possibly descibe the edge is that of a single free bosonic field. A gapless antiferromagnet - say the XXZ chain with anisotropy parameter Δ and Hamiltonian H_{XXZ},

$$H_{XXZ} = J \sum_i S_i^x S_{i+1}^x + S_i^y S_{i+1}^y + \Delta S_i^z S_{i+1}^z,$$

can be described using as the CFT of a *compactified* free bosonic field for a range of Δ, and we will find that our entanglement Hamiltonian can be as well.

The states of a CFT can be (in general) organized into irreducible representations of the Virosoro algebra, with each irrep featuring a 'heighest-weight' or primary state and a collection of descendants that can obtained from the primary state using operators in the algebra. In the plot of a finite size CFT spectrum, each primary field sits at the bottom of a *conformal tower*, and the descendant fields form a linear dispersion cone above it. We can see this pattern of linear dispersion for each charge sector in Figure 8. To make a precise comparison with the free-boson CFT, we'll need to solve for (or look up) the solution of this model.

The free-boson CFT is created from the Lagrangian

$$\mathfrak{L} = \frac{g}{2}\int dt \int_0^L dx(\frac{1}{v^2}(\partial_t\phi)^2 - (\partial_x\phi)^2)$$

and with the compatified field identification

$$\phi \equiv \phi + 2\pi R$$

and placed on the circle of circumference L with periodic boundary conditions

$$\phi(x) \equiv \phi(x + L).$$

After canonical quantization, it is found that the states of the free-boson CFT can be organized into irreps of the U(1) Kac-Moody algebra, an extended version of the Virosoro algebra which describes a left and right moving chiral current. Each Kac-Moody tower consists of an infinite number of Virosoro towers, so this greatly simplifies the description. The $U(1)$ Kac-Moody primaries $|e, m\rangle$ are labeled with a pair of integers e, m labeling the $U(1)$ charge and the winding number of the bosonic field respectively, and descendant fields (such as $\bar{\mathbf{j}}_{-\bar{n}}\mathbf{j}_{-n}|e, m\rangle$) are labeled additionally with a pair of non-negative integers $n, \bar{n}$ called the levels. The properties of the $U(1)$ Kac-Moody algebras constrain the form of energy and momentum eigenvalues - the eigenvalues are given in the table below in terms of the primary labels e, m and the levels $n, \bar{n}$.

$\mathbf{L_0}$	$2\pi g(\frac{e}{4\pi gR} + \frac{mR}{2})^2 + n$
$\bar{\mathbf{L}}_\mathbf{0}$	$2\pi g(\frac{e}{4\pi gR} - \frac{mR}{2})^2 + \bar{n}$
$\mathbf{P} = \frac{2\pi v}{L}(\mathbf{L_0} - \bar{\mathbf{L}}_\mathbf{0})$	$\frac{2\pi v}{L}(em + n - \bar{n})$
$\mathbf{H} = \frac{2\pi v}{L}(\mathbf{L_0} + \bar{\mathbf{L}}_\mathbf{0})$	$\frac{2\pi v}{L}(\frac{e^2}{4\pi gR^2} + \pi g m^2 R^2 + n + \bar{n})$
$\tilde{\mathbf{H}} = \frac{L}{2\pi v\kappa}\mathbf{H}$	$e^2 + \frac{m^2}{4\kappa^2} + \frac{1}{\kappa}(n + \bar{n})$

Table 1: Eigenvalues of states $|e, m\rangle_{n,\bar{n}}$. The rescaled Hamiltonian $\tilde{\mathbf{H}}$ has eigenvalues that depend on only one free-parameter, $\kappa = 1/(4\pi gR^2)$.(Note: A common convention is to set $g = 1/4\pi$ and describe the system using $R = \sqrt{1/\kappa}$.)

In addition, the bosonic CFT predicts that the state $\mathbf{j}_{-n}|e, m\rangle$ is degenerate with the states

$$\mathbf{j}_{-1}^n|e, m\rangle, \mathbf{j}_{-1}^{n-2}\mathbf{j}_{-2}|e, m\rangle, ... \prod_{i=1}^{\infty}\mathbf{j}_{-i}^{n_i}$$

where the total level is

$$\sum_{i=1}^{\infty} i * n_i = n.$$

This leads to a total degeneracy of $Z(n)*Z(\bar{n})$ for the level $n, \bar{n}$ descendants of $|e, m\rangle$ where $Z(n)$ is the number of partitions of the integer n. In particular, for chiral descendents with $\bar{n} = 0$, the first few degeneracies are $Z(n) = 1, 1, 2, 3$ for $n = 0, 1, 2, 3$.

The final line of Table 2.5 defines a rescaled Hamiltonian $\tilde{\mathbf{H}}$ whose eigenvalues only depend on the single dimensionless parameter $\kappa = 1/(4\pi gR^2)$, called the Luttinger parameter. By rescaling our entanglement spectra plots, we see that the entanglement Hamiltonian fits the form given for $\tilde{\mathbf{H}}$. These primaries are shown in Figure 13.

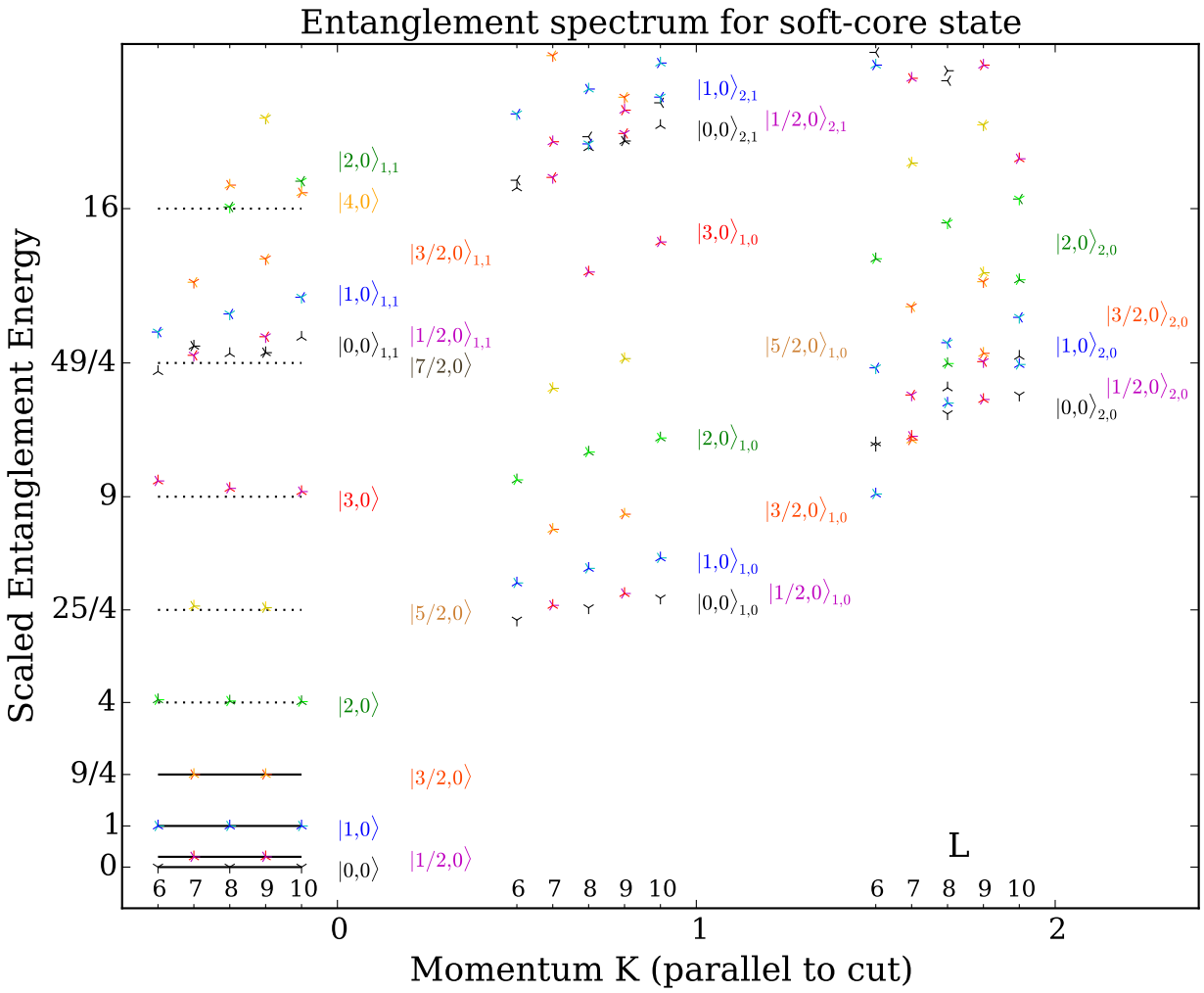

Figure 13: The identification of the states $|e,m\rangle_{n,\bar{n}}$ in the spectrum of the soft-core boson entanglement Hamiltonian. The label e gives the U(1) charge. The labels n, $\bar{n}$ label the levels in the right or left-moving sectors of the Kac-Moody algebra. When the level n is larger than 1, the level shows $Z(n)$ approximately degenerate states. The best estimate for the Luttinger parameter $\kappa = 1/6.4$ is given by the inverse of the energy of the $|1,0\rangle_{1,0}$ state. The label m is 0 for all states shown - however, the primary states $|e, m = \pm 1\rangle$ can be seen centered around momentum π, with energies on the order of $1/(4\kappa^2)$.

3 Appendix - Additional Figures

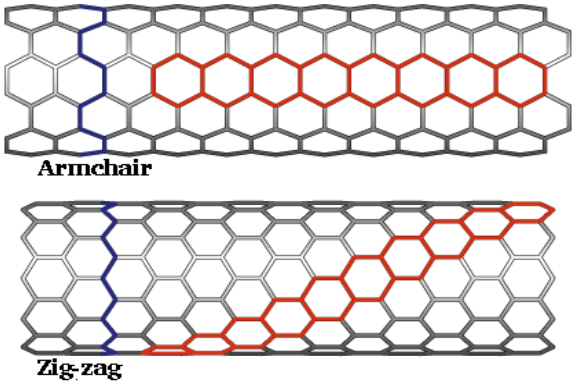

Figure 14: Zig-zag and armchair configurations of the honeycomb lattice on a cylinder

The below figures show the correlation functions for the soft-core and hard-core boson states, on a cylindrical honeycomb lattice in the zig-zag configuration, with circumference $L = 7$. See Figures 14 and 15.

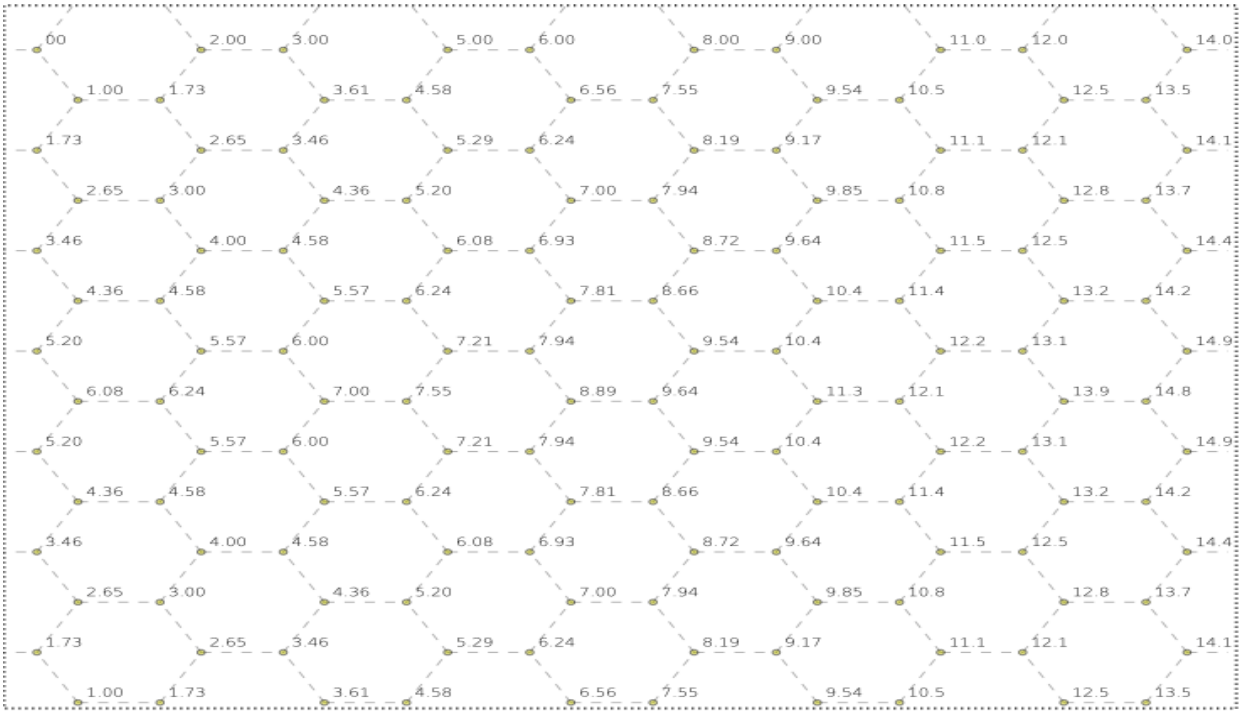

Figure 15: The zig-zag configuration used for the detailed correlation scatter plots below. Values are distances measured along the cylinder, using the shortest path and periodic boundary conditions in the y-direction.

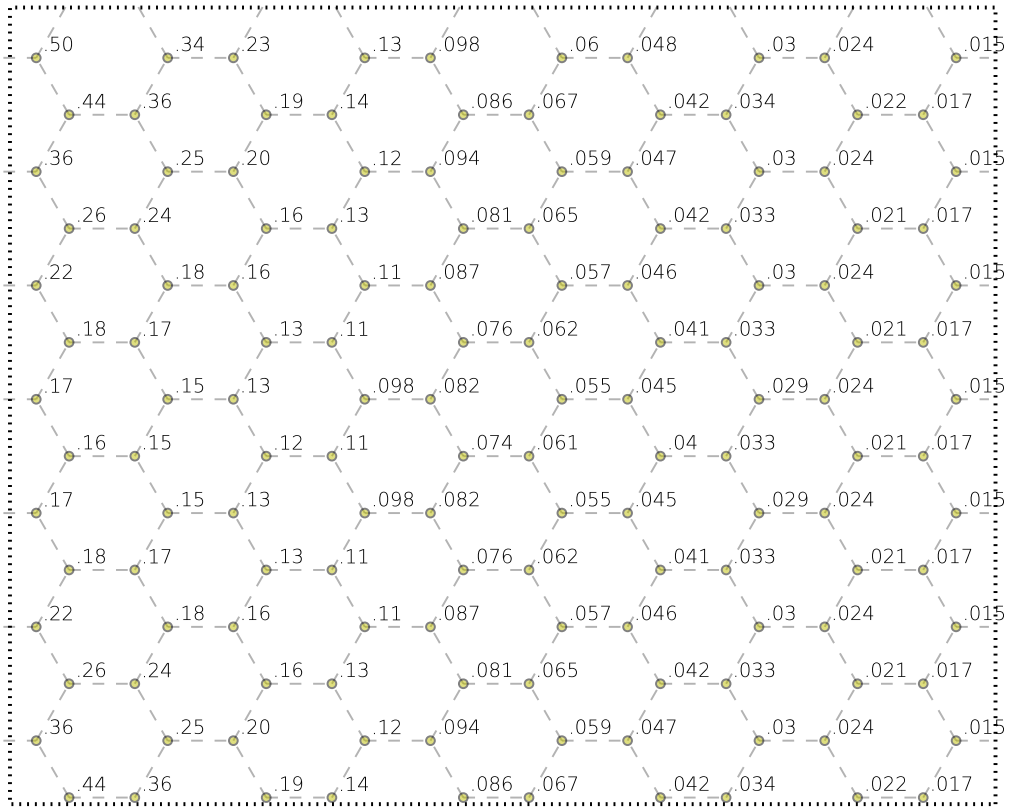

Figure 16: $< b_x b_0^\dagger >$ for soft-core boson state with $L = 7$. The subscripts 0, x refer to the position of the operators, with 0 being the site in the top-left corner. The correlation function approximately obeys rotational symmetry near the top-left site, despite boundary conditions that don't obey the rotational symmetry.

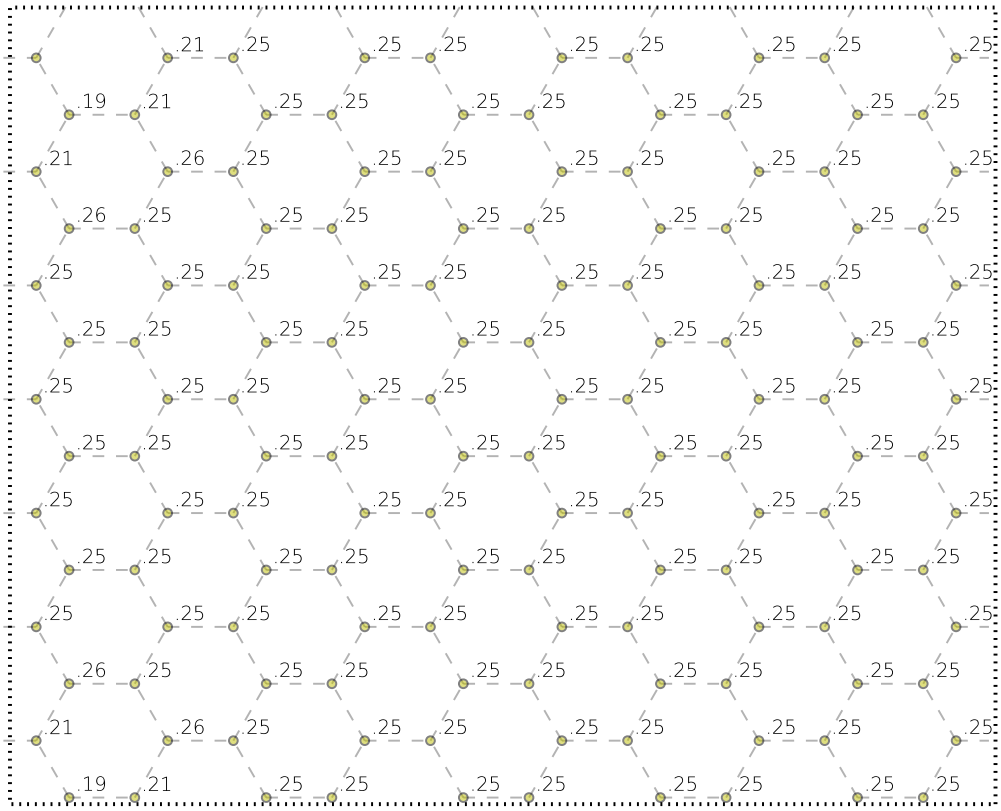

Figure 17: $< n_x n_0 >$ for soft-core boson state with $L = 7$. Due to the average boson density of $\frac{1}{2}$, the density-density correlation function asymptotes to $\frac{1}{4}$. The fluctuations around that mean decay very quickly.

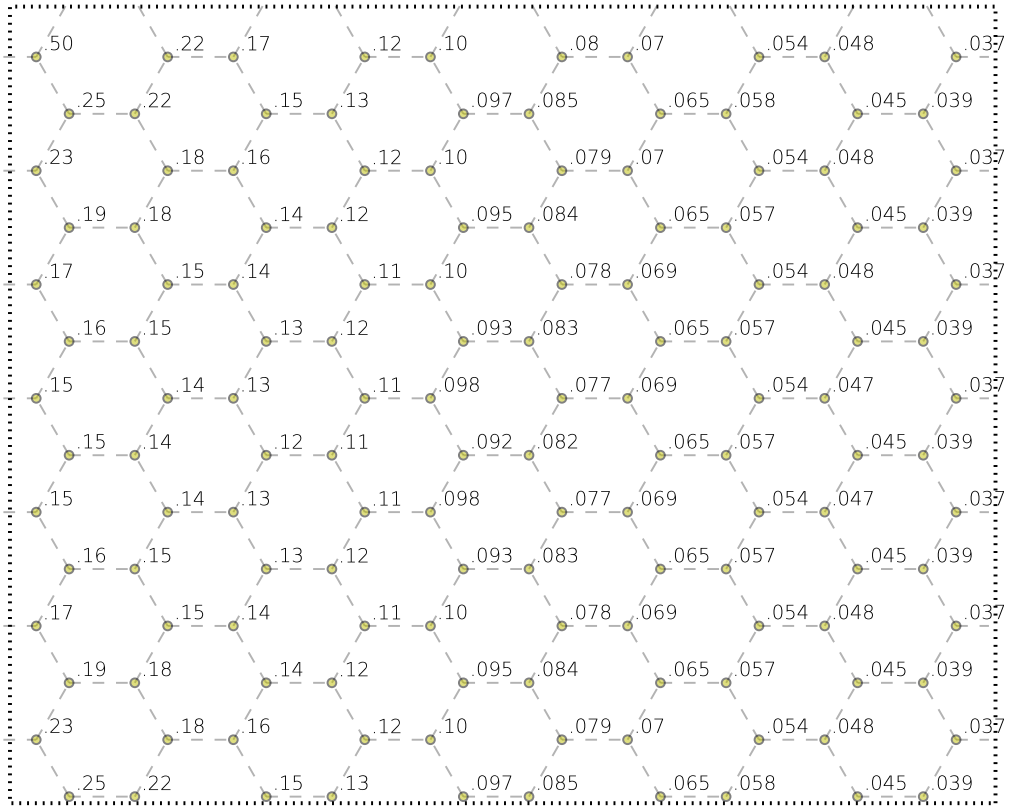

Figure 18: $< b_x b_0^\dagger >$ for hard-core boson state with $L = 7$. Compared to the soft-core boson state, short distance correlation values are less. The hard-core projection reduces the hopping amplitude due to the lack of available states to hop to if neighboring sites are filled. However, asymptotic decay of hopping is slower as you go down the cylinder, consistent with the increased MPS correlation length bound.

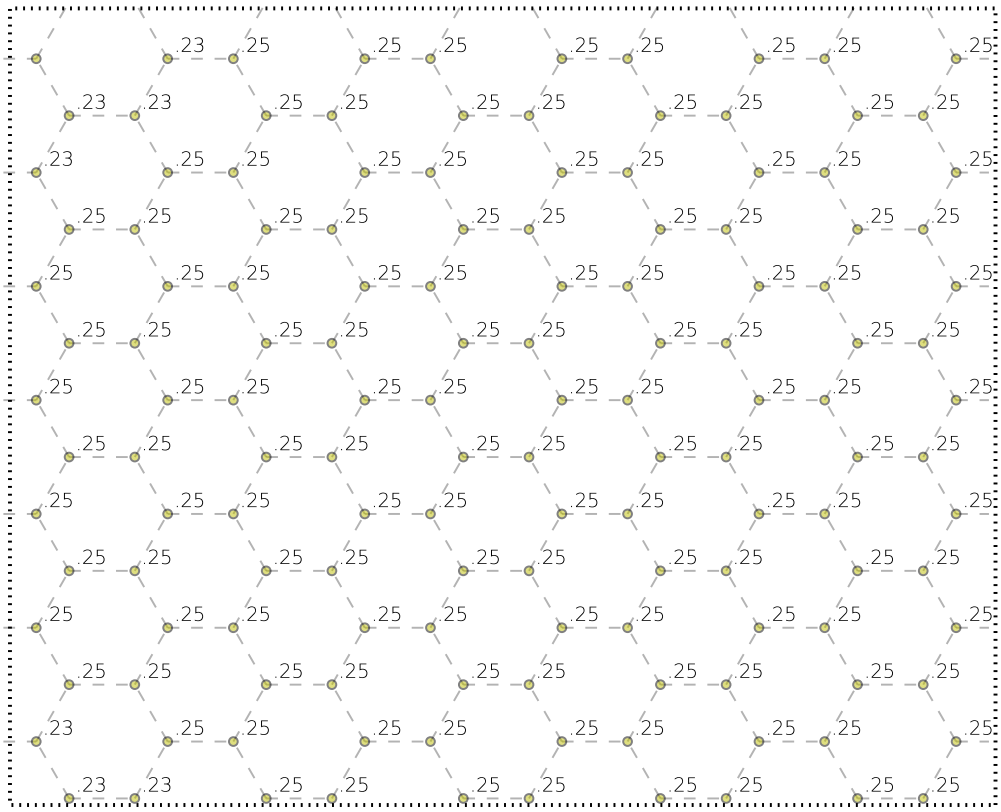

Figure 19: $< n_x n_0 >$ for hard-core boson state with $L = 7$.

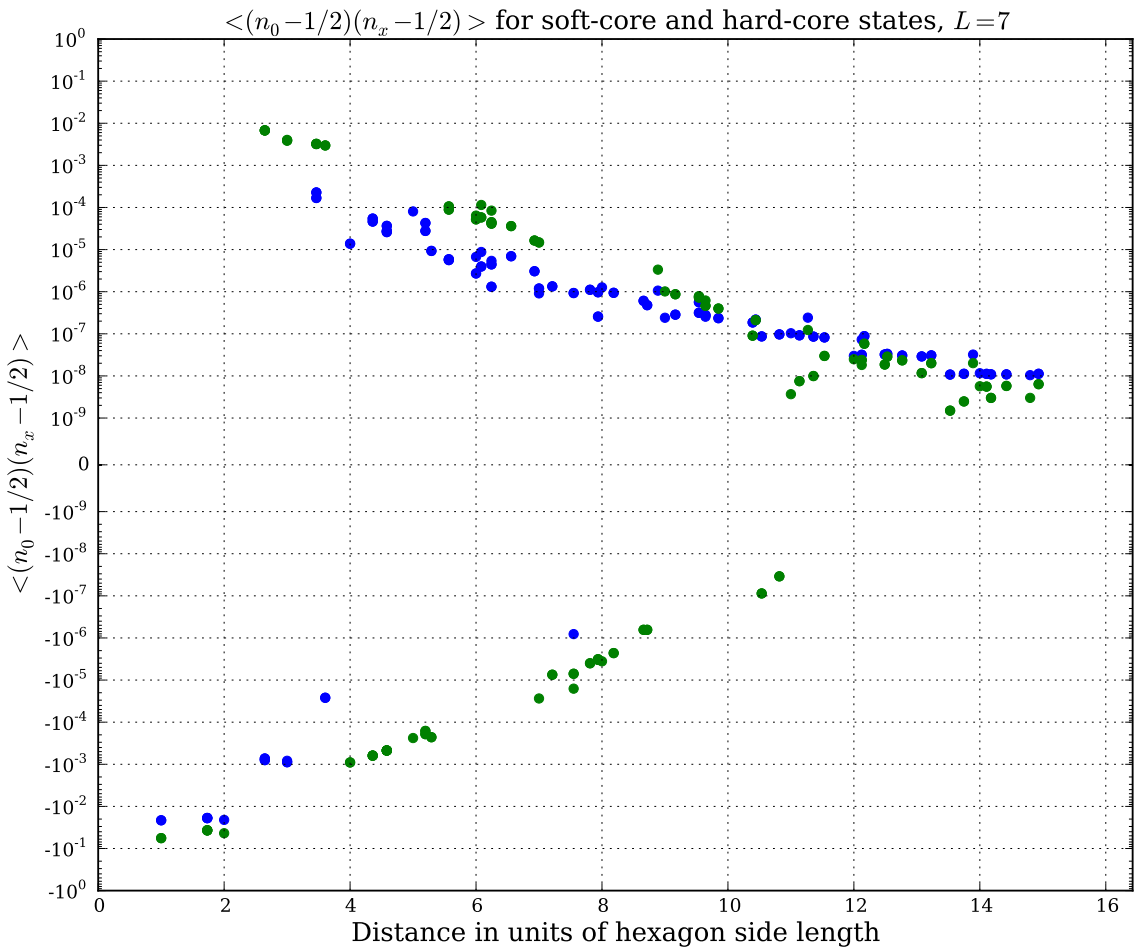

Figure 20: The connected density correlation function $< (n_x - \frac{1}{2})(n_0 - \frac{1}{2}) >$ shown on a log-scale for the hard-core (blue) and soft-core (green) boson states. The soft-core state shows some oscillation between positive and negative correlations in density fluctuations, while the hard-core state doesn't as much. Both density fluctuation correlation functions decay very quickly.

References

[1] J Ignacio Cirac, Didier Poilblanc, Norbert Schuch, and Frank Verstraete. Entanglement spectrum and boundary theories with projected entangled-pair states. 17 March 2011.

[2] Itamar Kimchi, S A Parameswaran, Ari M Turner, Fa Wang, and Ashvin Vishwanath. Featureless and non-fractionalized mott insulators on the honeycomb lattice at 1/2 site filling. 2 July 2012.

[3] D. Perez-Garcia, F. Verstraete, M. M. Wolf, and J. I. Cirac. Matrix Product State Representations. *eprint arXiv:quant-ph/0608197*, August 2006.